


# CO<sub>2</sub> capture and reduction to liquid fuels in a novel electrochemical setup by using metal-doped conjugated microporous polymers

Claudio Ampelli<sup>1</sup>  · Chiara Genovese<sup>1</sup> · Mina Errahali<sup>2</sup> · Giorgio Gatti<sup>2</sup> · Leonardo Marchese<sup>2</sup> · Siglinda Perathoner<sup>1</sup> · Gabriele Centi<sup>1</sup>

Received: 9 January 2015 / Accepted: 11 May 2015 / Published online: 16 May 2015  
© Springer Science+Business Media Dordrecht 2015

**Abstract** An electrochemical device for the reduction of CO<sub>2</sub> back to liquid fuels is here presented. The key of this novel electrocatalytic approach is the design and development of the gas diffusion membrane (GDM), which is obtained by assembling (i) a proton selective membrane (Nafion), (ii) a nanocomposite electrocatalyst based on metal-doped conjugated microporous polymer (CMP) and (iii) a C-based support working as the gas diffusion layer. CMP is a very attractive material able to adsorb CO<sub>2</sub> selectively with respect to other gases (such as H<sub>2</sub>, O<sub>2</sub>, N<sub>2</sub>, etc.), also in mild conditions (r.t. and atmospheric pressure). Particularly, tetrakis-phenylethene conjugated microporous polymer (TPE-CMP) was synthesized through Yamamoto homo-coupling reaction. TPE-CMP was modified by depositing noble (Pt) and non-noble (Fe) metal nanoparticles to create the active catalytic sites for the process of CO<sub>2</sub> reduction directly on the polymer surface where CO<sub>2</sub> is adsorbed. The metal-doped TPE-CMP electrocatalysts were fully characterized by infrared spectroscopy (IR), thermo-gravimetric analysis (TGA) and transmission electron microscopy (TEM). Then, the assembled GDM was tested in our homemade semi-continuous three-electrode electrochemical cell working in gas phase at 60 °C, coupled with a cold trap for the accumulation of the liquid products. Results showed the better

performances of the metal-doped TPE-CMP in terms of total productivity (C1–C8 oxygenates) with respect to other kinds of materials that do not show high CO<sub>2</sub> adsorption capacity.

**Keywords** CO<sub>2</sub> reduction · Solar fuels · Conjugated microporous polymers (CMP) · Pt and Fe nanoparticles

## 1 Introduction

The continuous increase of the carbon dioxide concentration, mainly due to the increased use of fossil fuels to meet the growing energy demand, has raised the attention on finding a sustainable solution to reduce the carbon emission [1]. Among the several strategies proposed, carbon capture and sequestration (CCS) is considered as crucial for meeting CO<sub>2</sub> emission reduction targets, as it is the only technology that may be implemented in a short term [2]. A CCS unit consists of a post-combustion installation that captures the carbon directly from the flue gas of a power plant [3]. Currently, there are three main separation options for post-combustion, based on the following technologies: (i) absorption, (ii) membranes and (iii) adsorption [4]. The latter option seems to be the most attractive in terms of cost effectiveness and it takes advantage of the gas adsorption capacity of some solid materials that preferentially adsorb CO<sub>2</sub> with respect to other gases (i.e. H<sub>2</sub>, N<sub>2</sub>, O<sub>2</sub>, etc.).

The main challenge regarding CCS is to reduce the overall cost by lowering both the energy and the capital cost requirements. For example, excellent separation performance can be achieved using amines as CO<sub>2</sub> absorbent but the regeneration step is an energy intensive process due to the strong binding of CO<sub>2</sub> to the amines. In general, adding a CCS system to a power plant reduces its

✉ Claudio Ampelli  
ampellic@unime.it

<sup>1</sup> Department of Electronic Engineering, Industrial Chemistry and Engineering, University of Messina, CASPE/INSTM and ERIC, V.le F. Stagno d'Alcontres, 31, 98166 Messina, Italy

<sup>2</sup> Department of Science and Technological Innovation, University of Piemonte Orientale, A. Avogadro, V.le T. Michel, 11, 15121 Alessandria, Italy

efficiency by as much as 30 %, including also the costs needed for CO<sub>2</sub> compression to 150 bar for storage, transportation and reuse [5]. An extremely promising strategy to reduce significantly costs and energy requirements, is to combine CO<sub>2</sub> removal with advanced carbon energy conversion [6]. In this context, the electrochemical reduction of CO<sub>2</sub> back to liquid fuels is a sustainable route to diminish the level of CO<sub>2</sub> in the environment [7, 8]. The technology consists of (i) adsorption of CO<sub>2</sub> on a conductive substrate and (ii) its catalytic conversion on metal-based active sites, starting from renewable sources (such as solar energy and water) [9]. The conversion of carbon dioxide and water into fuels in a “solar refinery” is a potential solution for reducing greenhouse gas emissions, but there are many technological advances that must be met in terms of capturing and sourcing the feedstocks (namely CO<sub>2</sub>, H<sub>2</sub>O and sunlight) and in catalytically converting CO<sub>2</sub> and H<sub>2</sub>O [10]. The main efforts of researchers, in fact, have been devoted to develop advanced materials able not only to adsorb CO<sub>2</sub> but also to catalyse its conversion to liquid fuels, better if high chain hydrocarbons and/or oxygenates favouring the formation of C–C bonds. However, it is also important to evaluate the engineering aspects of the process, by designing properly the configuration of the electrocatalytic device [11]. The realization of a solar refinery is contingent upon significant technological improvements in all those areas regarding the chemistry of the materials and the engineering of the electrocatalytic reactors. Particularly, there is the need to: (i) synthesize photoactive materials able to absorb efficiently sunlight [12, 13], (ii) develop novel advanced materials able to capture CO<sub>2</sub> [14], (iii) introduce the active phase for the catalytic conversion process [15] and (iv) design and realize (photo)electrochemical devices for a delocalized production of energy [16].

In the last years, different materials able to adsorb efficiently CO<sub>2</sub> have been developed: zeolites [17], alumina [18], metal organic framework (MOF) [19], covalent organic framework (COF) [20] and porous aromatic framework (PAF) [21, 22]. Yang et al. [23] prepared Mg-MOF-74 crystals showing high adsorption capacity and high isosteric heats of adsorption for CO<sub>2</sub>; their results confirmed excellent selectivity to CO<sub>2</sub> over N<sub>2</sub> at ambient conditions. Liu et al. [24] prepared a class of metal functional microporous covalent triazine frameworks using a metalloporphyrin as a single building block; the resulting polymer framework displayed excellent CO<sub>2</sub> uptake capacity at 273 K and 1 bar, depending on the porosity of the frameworks and functional activated sites in the skeletons. Recently, increasing attention has been turned to a new class of organic porous materials called conjugated microporous polymers (CMP) for their own characteristics, such as the intrinsic and unique combination of nanopores

and  $\pi$ -conjugated skeleton [25]. These materials are very promising because it is possible to modulate easily their specific properties and characteristics by changing the synthetic method and/or the building blocks [26, 27]. Due to their own microporosity coupled with the high surface area, CMP have largely been investigated for gas adsorption and storage purposes. The use of these materials in the reduction of CO<sub>2</sub> is a new area of development and there are only a few references in literature about their use as electrodes [28, 29]. The proper assembly of a multifunctional electrode (comprising a conductive substrate, an adsorbent support and the dispersed active sites) is of great and challenging importance to increase the productivity, efficiency and selectivity of the electrocatalytic CO<sub>2</sub> conversion process.

Among the different approaches of converting CO<sub>2</sub> to fuels, the most common option is based on a multistep sequence of (i) producing electricity using renewable energy sources (solar, wind, hydropower, etc.), (ii) then evolving H<sub>2</sub> by water electrolysis and (iii) using this hydrogen to produce chemical and fuels from CO<sub>2</sub> [30]. However, in a longer term vision it is necessary to integrate all these steps in a single photo-electrochemical (PEC) device able to use directly sunlight and convert the captured CO<sub>2</sub> and H<sub>2</sub>O to fuels such as methanol, methane and/or >C1 hydrocarbons and alcohols [31]. The PEC concept is based on the separation (with a membrane) of the photoelectrode for water oxidation (forming O<sub>2</sub>, protons and electrons) from the electrode for electrocatalytic reduction of CO<sub>2</sub> using the protons/electrons generated at the photoelectrode [32]. The separation of the two elements of the solar cell is necessary to avoid quenching phenomena between the reactive species and for safety aspects, related to the production of O<sub>2</sub> and fuels at the same place [33].

Another important aspect to consider is the recovery of the products of reaction. Conventional PEC devices operate in liquid phase, and most of the photo- and electrochemical studies were performed in liquid phase [34]. However, the recovery of the reaction products is often an energy intensive operation, which may eventually require more energy than the amount of renewable energy stored in the product of reaction. For this reason, it is fundamental that the solar PEC cell design includes the possibility for an easy recovery of the reaction products, for example operating the electrocatalytic reduction of CO<sub>2</sub> in a cell designed for gas phase and continuous operations and suitable for easy industrial scale-up [35]. Recent studies have demonstrated that, in order to overcome mass transport limitations and achieve high current densities, the preparation and optimization of the gas diffusion electrodes (GDEs) is the key to enhance mechanical stability and performance of the electrocatalysts in the reduction of CO<sub>2</sub>

[36]. The GDEs usually consist of a catalytic layer deposited on a gas diffusion layer by using binders, such as hydrophilic Nafion or hydrophobic polytetrafluoroethylene (PTFE) [37]. The GDEs for gas phase operation are also conceptually different from those used in the liquid phase. We employed GDEs analogous to those used in proton exchange membrane (PEM) fuel cells, but with a different electrocatalyst, based upon metal nanoparticles on polymer-based materials, which are able to convert CO<sub>2</sub> to >C1 alcohols and hydrocarbons.

In this context, we have analysed the feasibility of the electrocatalytic conversion of CO<sub>2</sub> to liquid fuels under gas-phase conditions, by using new conjugated microporous polymers as electrocatalysts. In particular, we synthesized tetrakis-phenylethene conjugated microporous polymer (TPE-CMP) and doped its surface with metal nanoparticles of noble (Pt) and not-noble (Fe) metals. We have tested their performances by using a homemade electrocatalytic cell, built in Plexiglas, by supplying controlled electric current and protons to the electrocathode. The combination of CO<sub>2</sub> capture and its transformation to industrial valuable compounds or fuels, may become one of the most important routes to reduce the CO<sub>2</sub> emission from power plants. The conversion of CO<sub>2</sub> back into fuels, in fact, may close its cycle of production/consumption, while the production of value-added products may diminish the use of fossil fuels needed for their production [38].

The mechanism of CO<sub>2</sub> reduction is very complex and involves multiple reaction pathways, which can lead to a large variety of products ranging from CO to various oxygenates such as alcohols, aldehydes and carboxylic acids. Between the different schemes proposed in literature [39], a common aspect refers to the presence of two main steps: (i) the reduction of CO<sub>2</sub> to give chemisorbed CO (through the formation of a carbon dioxide anion radical CO<sub>2</sub><sup>-</sup>) and (ii) the production of the formate anion or the further reaction of CO to give adsorbed :CH<sub>2</sub> species. Finally, coupling these :CH<sub>2</sub> species leads to the formation of C–C bonds and the production of longer chain hydrocarbons and this is favoured by operating in gas phase conditions, as discussed in the introduction section. The chain growing mechanism is similar to that occurring in Fisher-Tropsch process, even though both operating conditions and product distribution are very different with respect to our electrochemical system (we operate at relatively low temperature and in presence of electrical current). The C–C bond formation is one of the most critical factors to be taken into account in designing an electrocatalyst for the production of solar fuels. However, it is not still clear the rate determining step of the CO<sub>2</sub> reduction process. Increasing the number of CO<sub>2</sub> adsorption sites may be a favourable route to enhance productivity, especially if these sites are selective for CO<sub>2</sub>

with respect to other gases. It is well known that water electrolysis is the main side reaction of such kinds of electrochemical devices. Applying a bias between two electrodes (even if these were made of inert materials such as Pt, carbon, etc.) in presence of water, it unavoidably gives H<sub>2</sub> gas evolution and, even though our cathode operates in gas phase, water is present in the cathode side because it penetrates through the Nafion membrane from the anode (phenomenon assisted by the continuous CO<sub>2</sub> flow). The as-formed H<sub>2</sub> molecules that remain adsorbed on the electrocatalyst may reduce the production of high-chain hydrocarbons and oxygenates because they occupy the catalytic sites needed for CO<sub>2</sub> reduction. Thus, there is the need of advanced substrate materials which can:

- Adsorb high quantities of CO<sub>2</sub>, also in mild operating conditions (low temperature and pressure);
- Be selective to CO<sub>2</sub> adsorption than other gases (i.e. H<sub>2</sub>);
- Allow a good dispersion of active metal nanoparticles on their surface;
- Have a co-catalytic role in CO<sub>2</sub> reduction.

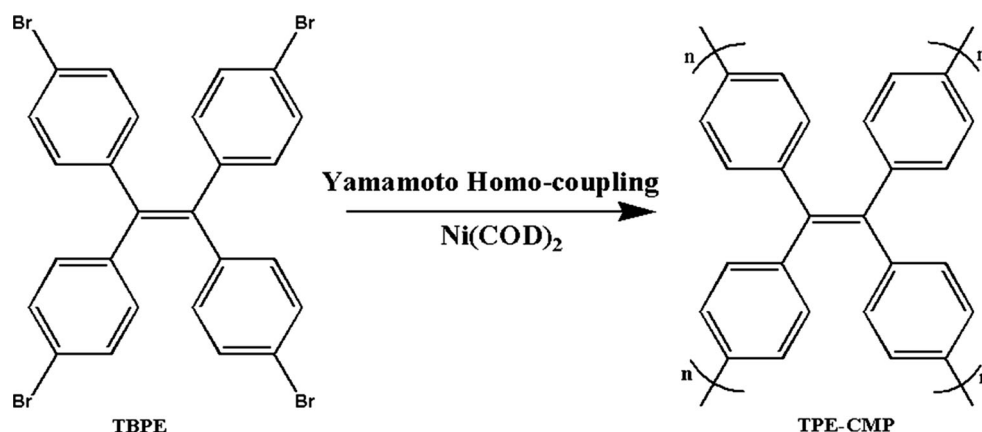
In this context, we prepared conjugated microporous polymers, which seem good candidates as substrates for the electrocatalytic reduction of CO<sub>2</sub> to produce liquid fuels. The key aspect to improve the overall efficiency is not only the preparation of the electrocatalyst (doped with suitable metals) but also the capability to assemble the electrode materials to form a multilayered composite to guarantee good proton mobility and electron conductivity.

## 2 Experimental

### 2.1 Preparation of the electrode

TPE-CMP was synthesized using the Yamamoto coupling following the procedure reported by Xu et al. [26]. In particular, 1,5-cyclooctadiene (COD, 1.05 mL, 8.32 mmol) was added to a solution of bis(1,5-cyclooctadiene)nickel(0) [Ni(cod)<sub>2</sub>, 2.25 g, 8.18 mmol] and 2,2'-bipyridyl (1.28 g, 8.18 mmol) in anhydrous DMF (120 mL) and the mixture was heated under Ar at 353 K for 1 h. 1,1,2,2-Tetrakis(4-bromophenyl)ethene (TBPE) (1 g, 1.54 mmol) was added to the resulting purple solution and the mixture was stirred at 353 K overnight to obtain a deep purple suspension. After cooling to room temperature, concentrated HCl was added to the mixture. After filtration, the residue was washed with H<sub>2</sub>O (5 × 30 mL), THF (5 × 30 mL) and CHCl<sub>3</sub> (5 × 30 mL) and dried in vacuum to give a yellow powder (90 % yield). Figure 1 shows a schematic representation of TPE-CMP formation.

**Fig. 1** Schematic representation of TPE-CMP formation



Then, 10 wt% Pt (or Fe) were deposited on TPE-CMP by sol immobilization technique [40] using  $K_2PtCl_4 \cdot 2H_2O$  (or  $FeNO_3 \cdot 2.5H_2O$ ) as precursor,  $NaBH_4$  as reducing compound and PVA as protective agent. The solution (after acidification at  $pH = 2$ ) was added to the support under vigorous stirring. The powder was filtered, washed until neutral  $pH$  and finally dried at  $80^\circ C$  for 4 h. As reference materials, commercial multiwalled carbon nanotubes purchased from Applied Science (CNTs, Pyrograph<sup>®</sup>-III, PR24) were also tested. Pt (or Fe) was deposited on CNTs by incipient wetness impregnation starting from an ethanol solution containing the same metal precursors used to dope TPE-CMP. After drying at  $60^\circ C$  for 24 h, the samples were annealed for 2 h at  $350^\circ C$  and reduced in  $H_2$  at  $400^\circ C$  for 2 h. The final metal loading was 10 wt%.

## 2.2 Characterization

The electrocatalytic materials were fully characterized using different techniques. The Infrared (IR) spectra of the materials in KBr pellets were collected using a Bruker Equinox 55 Spectrometer equipped with a pyroelectric detector (DTGS type) with a resolution of  $4\text{ cm}^{-1}$ . The same instrument was used for collecting Diffuse Reflectance Infrared spectra (DRFTIR); in this case, the instrument was equipped with a commercial DRFTIR Thermo Electron Corporation cell Collector<sup>TM</sup> equipped with Si windows, the spectra were recorded with  $4\text{ cm}^{-1}$  resolution and the materials were used without any pelletisation pretreatment. The cell was permanently attached to a vacuum line (residual pressure  $1 \times 10^{-3}$  mbar), allowing all outgassing pretreatments and  $CO_2$  adsorption-desorption experiments to be carried out in situ.

Spectra of  $CO_2$  adsorbed on materials have been collected at beam temperature (ca.  $35^\circ C$ ) on samples, previously dehydrated under vacuum at beam temperature for 1 h, using a maximum pressure of  $CO_2$  of 80 mbar.

The Thermogravimetric analysis (TGA) was performed on a Setaram SETSYS Evolution instrument under argon (gas flow  $20\text{ mL/min}$ ), heating the samples up to  $1373\text{ K}$  with a rate of  $2\text{ K min}^{-1}$ . Transmission Electron Microscopy (TEM) images were acquired by using a Philips CM12 microscope (resolution  $0.2\text{ nm}$ ) with an accelerating voltage of  $120\text{ kV}$ . Nitrogen physisorption measurements were carried out at  $77\text{ K}$  in the relative pressure range from  $1 \times 10^{-7}$  to  $1\text{ P/P}_0$  by using an Autosorb iQ/ASiQwin instrument (Quantachrome instrument). Prior to the analysis, the samples were outgassed at  $150^\circ C$  for 16 h (residual pressure lower than  $10^{-6}$  Torr). Specific surface areas were determined using the Brunauer–Emmett–Teller (BET) equation, in the relative pressure range from 0.05 to  $0.15\text{ P/P}_0$ . Pore size distributions were obtained by applying the NLDFT (non-local density functional theory) method and using a silica model with cylindrical pore.

## 2.3 Assembly

An ethanol suspension of metal-doped TPE-CMP was impregnated on a commercial carbon-based nonwoven gas diffusion layer (GDL, SIGRACET 24BC, supplied by SGL Group). The main properties of the GDL are reported as follows:  $235\text{ }\mu\text{m}$  thickness,  $100\text{ g/m}^2$  areal weight, 76 % porosity,  $0.6\text{ cm}^3/(\text{cm}^2\text{ s})$  air permeability,  $<12\text{ m}\Omega\text{ cm}^2$  electrical resistance (through plane). In some experiments, the TPE-CMP was initially mixed with a little amount of CNTs, to increase the conductivity of the final electrode. In these cases, the active phase (namely Pt or Fe nanoparticles) was alternatively deposited on the surface of either TPE-CMP or CNTs, to understand the influence of metal localization (with respect to the actual sites of  $CO_2$  adsorption) on the process performances.

The working electrode was formed by assembling the metal-doped TPE-CMP(CNTs)/GDL with a Nafion<sup>®</sup> membrane (Nafion<sup>®</sup> 115, by Sigma Aldrich) by hot-

pressing at 80 atm and 130 °C for 90 s, finally having the active composite material (metal -doped TPE-CMP and/or CNTs) between the two layers (GDL and Nafion), to form a gas diffusion membrane (GDM). The active area of the electrode was 1 cm<sup>2</sup>, with a final metal loading of about 0.5 mg cm<sup>-2</sup>.

## 2.4 Experimental apparatus

Tests of CO<sub>2</sub> reduction were performed in gas phase by using a homemade semi-continuous electrochemical cell, built in Plexiglas and located inside an oven to operate at 60 °C. The cell has a three-electrode configuration, with a Pt wire (as counter-electrode) and a saturated Ag/AgCl electrode (as reference electrode) immersed in the anode part. The photo-generated current was simulated by applying a constant small bias through the cell to provide the electrons necessary for the CO<sub>2</sub> reduction process. The photo-anode was replaced by a compartment filled with a liquid electrolyte solution to act also as a source of protons (KHCO<sub>3</sub> 0.5 M). Figure 2 reports a schematic drawing of the experimental apparatus and assembly of the layers forming the GDM.

The anode, which operates in liquid phase, is only in contact with one side of the Nafion membrane, being the other side assembled with the GDL. The cathode, directly in contact with the free side of GDL, operates in gas phase under a constant flow of CO<sub>2</sub> (10 mL min<sup>-1</sup>). CO<sub>2</sub> can: (i) permeate through the GDL, (ii) reach the metal-doped TPE-CMP, (iii) adsorb on the polymer surface and (iv) react on the metal nanoparticles (Pt or Fe) to produce liquid fuels.

A potentiostat/galvanostat (Amel mod. 2049A) was used to supply a constant current (10 mA) between the

electrodes. Experiments were conducted in galvanostatic mode, inverting after 1 h the current polarity to improve desorption of the products from the working electrode. The voltage increases as a function of time-on stream during the first hour stabilizing to a value of about -1.5 V. Tests were also performed applying a constant potential (-1.5 V) and reading the generated current (potentiostatic mode), but the results were not significantly different. The analysis of the products of the reaction, collected in a cold trap, was performed by a gas-chromatograph equipped with a mass detector (Thermo Scientific GC Trace 1310—ISQ MS).

## 3 Results and discussion

### 3.1 Characterization of the electrocatalyst

The electrode materials were fully characterized by different techniques to understand their structural and morphological properties in relation with their capability of adsorbing CO<sub>2</sub> and reacting in the process of CO<sub>2</sub> reduction.

The IR spectrum of the as-synthesized polymer confirms the successful synthesis of the polymer. Figure 3 shows a comparison between the spectra of the TPE-CMP polymer (curve *b*) and the starting monomer TBPE (curve *a*).

Analysing the TBPE spectrum, bands with different intensities corresponding to the absorption characteristic of aromatic rings are present in the low frequency region. The bands at 1491 and 1444 cm<sup>-1</sup> involve “semicircle stretching pair” modes of the aromatic rings. The intense and sharp band at 1004 cm<sup>-1</sup> is assigned to the C–C bending of the aromatic rings coupled with C–H bending.

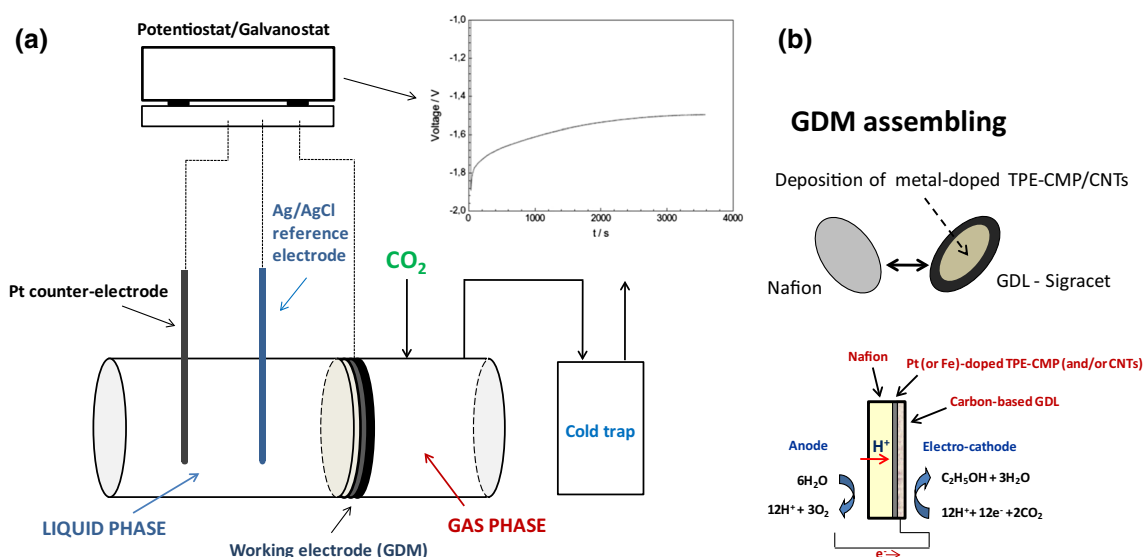


**Fig. 2** Schematic drawing of the **a** electrochemical device for the gas-phase CO<sub>2</sub> reduction and **b** Gas diffusion membrane (GDM) assembly

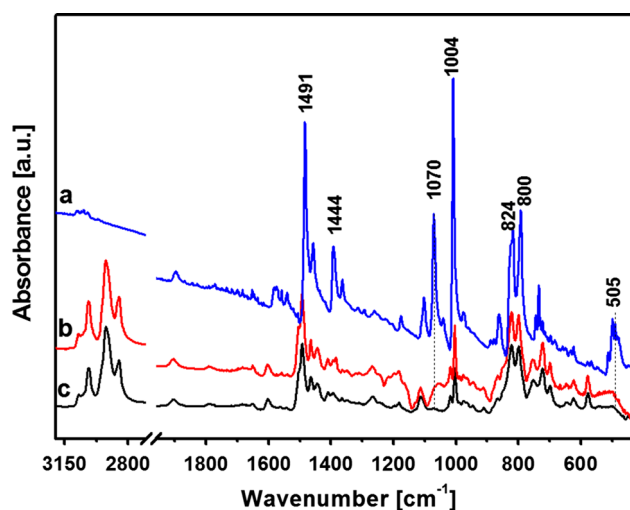


**Fig. 3** IR spectra in the region 3200–400  $\text{cm}^{-1}$  of TBPE monomer (curve *a*), TPE-CMP polymer (curve *b*) and Pt-doped TPE-CMP (curve *c*) in KBr pellets

The absorption bands at 824 and 800  $\text{cm}^{-1}$  are assigned to the ring and C–H out of plane bending. All these modes are maintained in the TPE-CMP polymer. The disappearance of the bands of the C–Br vibrations at 1070 and 505  $\text{cm}^{-1}$  in the TPE-CMP spectrum indicates the cleavage of C–Br bonds and the successful formation of the phenyl–phenyl coupling. The electrocatalyst material (Pt-doped TPE-CMP) spectrum is also reported in Fig. 3 (curve *c*). As it can be seen, the structural vibrational modes of the starting material (curve *b*) have not undergone any modification, even after the sol immobilization treatment and the subsequent annealing.

Another important characterization is the FTIR  $\text{CO}_2$  adsorption made in situ at room temperature, because it gives information about the type of interactions involved between the  $\text{CO}_2$  molecule and the electrocatalytic material.

The interactions of  $\text{CO}_2$  with TPE-CMP (Fig. 4a) and Pt-doped TPE-CMP (Fig. 4b) were investigated using the diffuse reflectance infrared spectroscopy. In Fig. 4a, curve *a* refers to the spectra of  $\text{CO}_2$  in gas phase.

The gaseous  $\text{CO}_2$  is a linear molecule with two infrared active absorption bands at 2349  $\text{cm}^{-1}$  ( $\nu_3$  antisymmetric stretching mode) and 667  $\text{cm}^{-1}$  ( $\nu_2$  bending mode) [41].

In order to clarify the data, the curves are shown in subtraction mode, as the curve of the material before interaction with  $\text{CO}_2$  has been subtracted from the original curves recorded after dosage of different pressures of  $\text{CO}_2$ .

Upon exposure of TPE-CMP to  $\text{CO}_2$ , a positive absorption band at 2334  $\text{cm}^{-1}$  appeared in the difference spectrum (Fig. 4a, curve *b*) with a shoulder at 2322  $\text{cm}^{-1}$ . After progressive outgassing, all the component peaks in the spectrum disappeared. If compared with the spectra of

$\text{CO}_2$  gas phase, all the curves show the presence of the gas phase in the spectra.

Upon interaction with the surface, the molecules can attach to the surfaces in physisorption or chemisorption ways. The first way is a van der Waals interaction between the adsorbate and the substrate. In the second, the adhesion occurs with the formation of a chemical bond. Infrared spectroscopy can be used to distinguish between these two mechanisms because only a slight shift in the absorption band frequency accompanies physisorption, whereas chemisorption is accompanied by a much larger shift to lower energy.

Physisorbed  $\text{CO}_2$  on carbon-containing surfaces such as C60, graphite, diamond and carbon [42, 43] has been reported to display absorption bands between 2340 and 2323  $\text{cm}^{-1}$  for the  $\nu_3$  antisymmetric stretching mode. The presence of a distinct narrow band at 2334  $\text{cm}^{-1}$  suggests that there is one type of sorption site for the  $\text{CO}_2$  in the TPM-CMP material. The shoulder absorption band at 2322  $\text{cm}^{-1}$  has been reported for  $\text{CO}_2$  interacting with polymers [44], carbon nanotubes [45], and should be a combination mode or a different adsorption site in the materials; the intensity ratio between the band at 2334 and 2322  $\text{cm}^{-1}$  was maintained for all the pressures (Fig. 4, curve *b*–*q*) and this fact suggests that the band at 2322  $\text{cm}^{-1}$  could be related to a combination mode.

Figure 4b shows the analysis of Pt-doped TPE-CMP material after interaction of 80 mbar of  $\text{CO}_2$ . In this case, the component at 2349  $\text{cm}^{-1}$  related to the adsorption of  $\text{CO}_2$  gas phase has a similar intensity in comparison of the analogous spectrum of TPE-CMP material. On the other hand, a reduction of the intensity of the bands at 2334 and 2322  $\text{cm}^{-1}$  should be associated at a lower specific surface area of the materials after the thermal treatment during the addition of platinum phase or a partial closure of the pores caused by the presence of nanoparticles of Pt.

In order to understand the nature of the interaction between the Pt-doped TPE-CMP and  $\text{CO}_2$  molecules, it is possible observing the region at lower energy in which a band at about 669  $\text{cm}^{-1}$  ( $\nu_2$  bending mode) of  $\text{CO}_2$  gas phase is present, and new absorption bands at 659 and 650  $\text{cm}^{-1}$  appeared as broad bands shifted to lower frequency from the gaseous  $\text{CO}_2$  (Fig. 4b, inset). The shift frequency of 10 and 19  $\text{cm}^{-1}$  respectively are comparable with the shift induced by interaction with of phenyl ring [44] and this suggests that, also in the case of Pt-doped TPE-CMP material, the principal interaction is a physisorption and  $\text{CO}_2$  has a good interaction with phenyl rings of the material structure.

Thermogravimetric Analysis (TGA) reported in the Fig. 5 shows the comparison between TPE-CMP material and Pt-doped TPE-CMP electrocatalytic material.

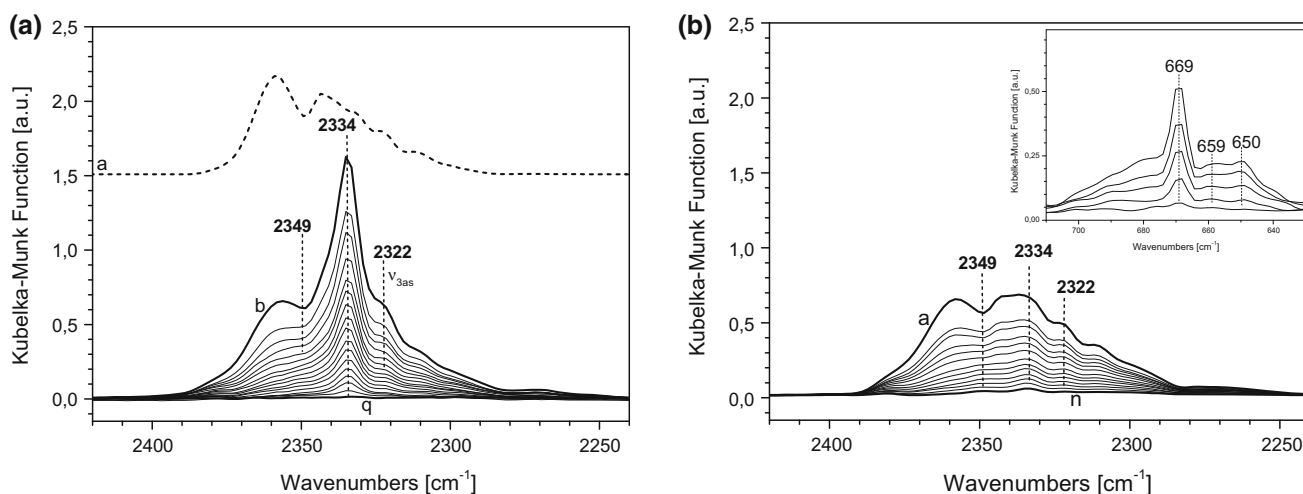


**Fig. 4** Diffuse reflectance infrared spectra of CO<sub>2</sub> gas phase (80 mbar) (a); TPE-CMP (a) and Pt-doped TPE-CMP (b) after dosage of 80 mbar of CO<sub>2</sub> and subtraction of the spectrum of the original material (b) and progressively outgassing (c–q; a–n); residual pressure  $1 \times 10^{-3}$  mbar

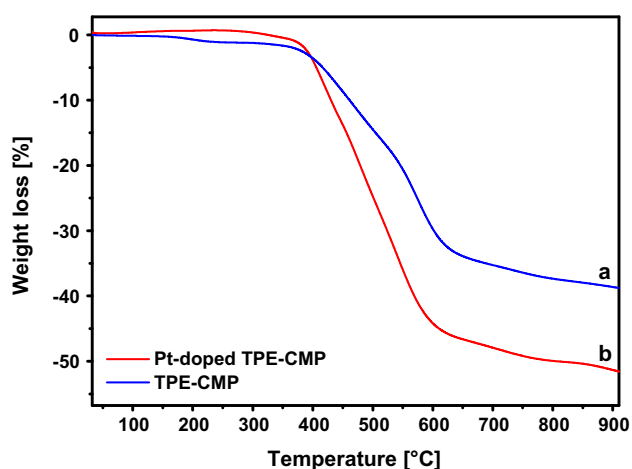


**Fig. 5** TGA plots of TPE-CMP *a* and Pt-doped TPE-CMP *b* samples, run under argon atmosphere up to a maximum temperature of 900 °C

TGA confirmed the good thermal stability of the starting support TPE-CMP (curve *a*). The decomposition of the polymer begins at approximately 350 °C. This high thermal stability allows the maintenance of the properties of the polymer during the preparation of the electrocatalytic material (curve *b*) which shows a similar thermal stability.

The material porosity was analysed by adsorbing gases at low temperature: N<sub>2</sub> adsorption/desorption isotherms were collected at 77 K (Fig. 6a). The isotherm of TPE-CMP polymer can be classified as type I, with gradual filling of mesopores also indicated by formation of hysteresis loop in the desorption branch. Whereas, after the formation of electrocatalyst phase, the isotherm is characterized by a Langmuir profile, without mesoporosity. The apparent BET surface areas were calculated over a relative pressure range  $P/P_0 = 0.05\text{--}0.15$ .

The BET surface area for TPE-CMP is 850 m<sup>2</sup>/g, which decrease to 360 m<sup>2</sup>/g for Pt-doped TPE-CMP.

Figure 6b shows the pore size distribution for the TPE-CMP material compared with Pt-doped TPE-CMP calculated using nonlocal density functional theory (NLDFT) on silica surface with cylindrical geometry applied in the desorption branch.

The starting polymer mainly exhibits a meso and macroporous distribution centred at 55 Å. Instead, the polymer Pt-doped TPE-CMP is characterized by microporous pores at 10 Å and small mesoporosity with respect to the starting polymer.

The surface area of the starting polymer decreases, as expected, after treatment which led to the formation of the electrocatalyst material. The reduction of the starting mesoporosity is due to the presence of Pt which grows inside of the pores and reduces the dimension of mesopore obtaining a predominant microporosity in the Pt-TPE-CMP material. This is in good agreement with IR spectroscopy that indicates a reduction of the total specific surface area, but at the same time a strong affinity between CO<sub>2</sub> and material surface.

The reduction of the meso- and macroporosity between 50 and 200 Å does not affect the performance of the system, because in this type of pore the CO<sub>2</sub> interaction with the material surface is very weakly. On the other hand, the new microporosity will bring a better interaction and storage of CO<sub>2</sub> and consequently will increase catalytic activity of the electrocatalytic material.

Transmission electron microscopy (TEM) was used to determine the metal particle size distribution and characteristics of the electrocatalysts. Figure 7 shows the results for Pt-doped TPE-CMP. Platinum nanoparticles are well visible in high contrast with respect to the polymer surface

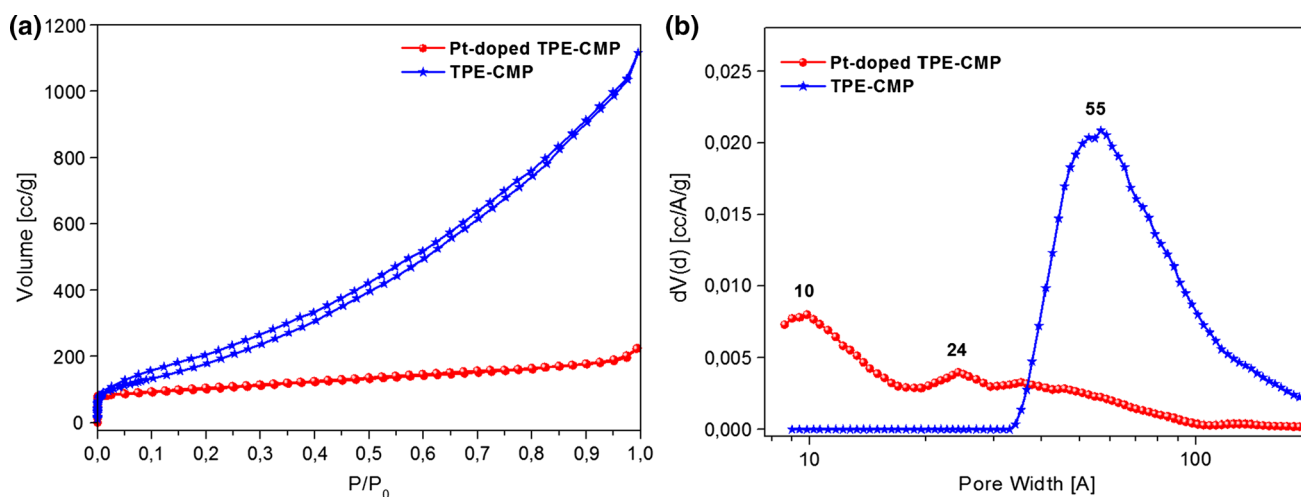
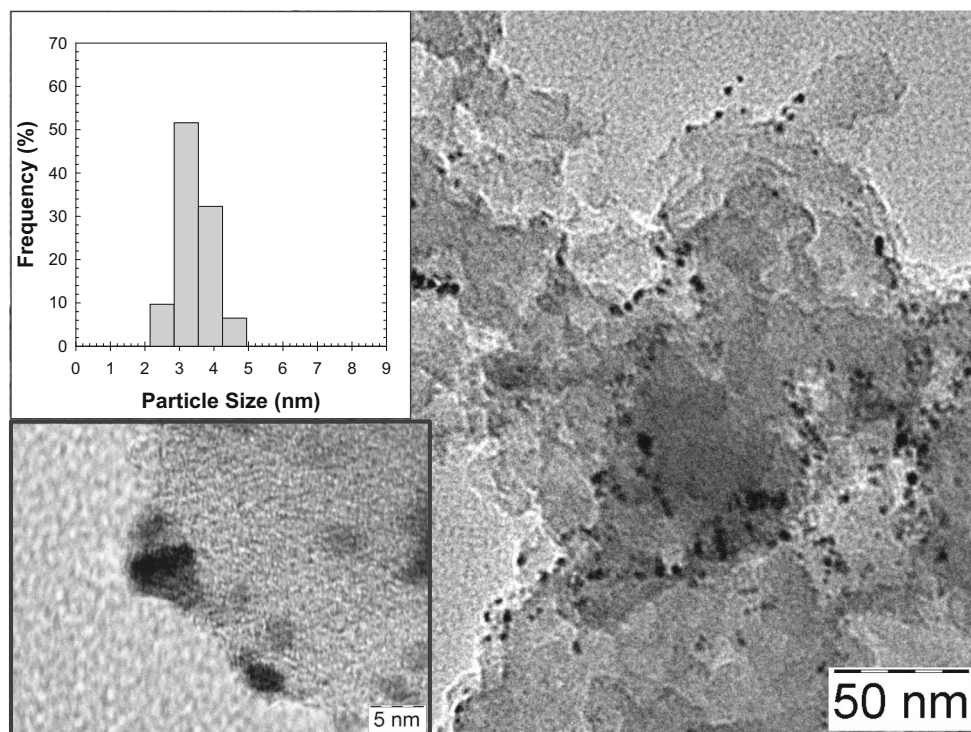


**Fig. 6** N<sub>2</sub> physisorption isotherms (a) and pore size distribution (b) of the TPE-CMP (*stars*) and Pt-doped TPE-CMP (*spheres*)

**Fig. 7** Representative TEM images of Pt-doped TPE-CMP electrocatalyst with the relative estimated metal particle size distribution



and show a relatively narrow size distribution (in the 2.5–4.7 nm range), with an average particle diameter of 3.5 nm. Moreover, they are well dispersed over the TPE-CMP surface and no abnormally large particles or aggregates were observed. The inset on the same figure shows some Pt nanoparticles in high resolution, presenting a slightly elongated shape.

Figure 8, instead, shows the TEM results for Fe-doped TPE-CMP. Iron particles are much larger than platinum particles. The metal particle size distribution, not reported here, is very broad with diameter from 10 to 30 nm.

Though they are well dispersed over the TPE-CMP surface, aggregates of 10–15 nm particles are also present.

### 3.2 CO<sub>2</sub> reduction testing

The as-prepared assembled electrodes were tested in the process of CO<sub>2</sub> reduction by using our lab-scale electrochemical device, described in the experimental part. Nonetheless, it is worth it to remember that we operated in gas phase, exposing the electrocatalyst to a continuous CO<sub>2</sub> gaseous stream. The reaction mechanism is probably quite



different comparing gas and liquid phase conditions. Most of the electrocatalytic cells reported in literature work in liquid phase, showing several issues mainly related to  $\text{CO}_2$  solubility. To increase the  $\text{CO}_2$  supply direct to the surface of the electrocatalyst, some researchers investigated liquid  $\text{CO}_2$  reduction at high pressure (at about 60 bar) [46]. Comparing to those results, the kinds of products that we obtained ( $C > 1$  alcohols and oxygenates) are very similar. This suggests that there is a parallelism between the operating conditions that we adopted (solvent-free at 1 atm) and high pressure operation in liquid electrolyte, which is conditioned from the low solubility of  $\text{CO}_2$ . Figure 9 shows

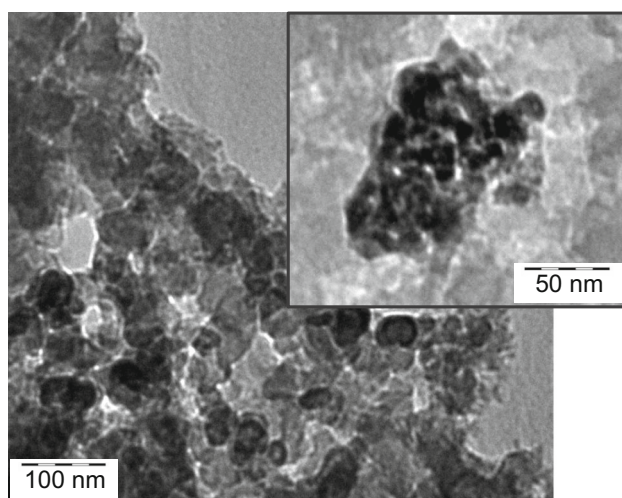


**Fig. 8** Representative TEM images of Fe-doped TPE-CMP electrocatalyst

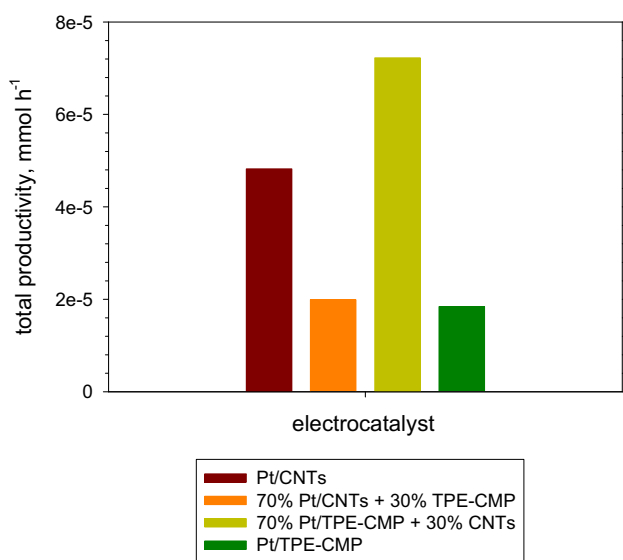


**Fig. 9** Total productivity obtained in the gas-phase  $\text{CO}_2$  reduction process using Pt-doped TPE-CMP or Pt-doped CNTs (or a combination of the two systems) as electrocatalysts

the experimental results in terms of total productivity for Pt/TPE-CMP electrocatalysts. For total productivity we mean the sum of the liquid products (C1–C8 oxygenates, mainly alcohols ranging from methanol to octanol) produced in 1 h of testing experiment.

Pt-doped CNTs were also tested in the  $\text{CO}_2$  reduction process and considered as a reference material, as we already know their electrocatalytic behaviour [8, 11]. Moreover, in the same graph we reported testing results obtained by mixing TPE-CMP with CNTs. To deposit the electrocatalytic material on the GDL, before assembling with the Nafion membrane to form the GDM, a homogeneous ink of TPE-CMP in ethanol was used for the impregnation. Due to the own characteristics of TPE-CMP, the preparation of the ink was critical and then we mixed the polymer with 30 wt% of CNTs improving the quality of the ink and obtaining a workmanlike deposition. Results show the increasing performances in terms of productivity of the Pt-doped TPE-CMP mixed with CNTs. The presence of microporous conjugated polymers enhanced the process performances due to their intrinsic porosity and high  $\text{CO}_2$  adsorption capability that increase the local concentration of  $\text{CO}_2$  close to the catalytic sites (Pt nanoparticles). A proper assembly of the electrocatalytic layers is very important to guarantee a good proton mobility and a high electron conductivity. Among the other polymers able to adsorb selectively  $\text{CO}_2$  (zeolites, alumina, MOF, COF, etc.), conjugated microporous polymers (CMP) show properties of electric conductivity, resulting as potential substrate materials for electrocatalytic applications. Mixing TPE-CMP with CNTs further increases the electronic conductivity of the electrode improving the transport of electrons (coming from the photo-anode, or provided from the potentiostat in the actual testing experiments) to the metal nanoparticles deposited on the substrate. Probably, doping of the TPE-CMP with active metals is not sufficient to increase the productivity compared to Pt on CNTs due to a loss of conductivity. However, it was sufficient to add a small amount (30 wt%) of CNTs to increase considerably the productivity. Thus, the positive effect in mixing the polymer with CNTs is doubled: (i) improved quality of the ink for a better dispersion on the GDL and (ii) enhanced conductivity of the electrode.

Another aspect that we analysed was the effect of localization of the Pt nanoparticles over the substrate. Particularly, we tried to mix Pt-doped CNTs with 30 wt% of pure polymers (TPE-CMP). In this case, it can be observed that there is a worsening in the total productivity with respect to the reference sample, probably due to a dilution effect of the active phase with respect to the reference (Pt-doped CNTs 100 %). We may conclude that is of great importance the localization of the active phase (Pt), which should be deposited on the polymer surface where  $\text{CO}_2$

adsorption occurs. This may help in the definition of the tentative reaction mechanism: as there is accordance that nanocarbons (such as CNTs) may also play co-catalytic roles in different catalytic applications [47], this hypothesis suggests that the rate determining step could be the formation of the carbon dioxide anion radical  $\text{CO}_2^-$ , as the CNTs are probably involved in the second step influencing the kinds of liquid products for their confinement effect. Figure 10 shows the product distribution for the same series of Pt-doped TPE-CMP/CNT electrocatalysts in the gas  $\text{CO}_2$  reduction process. Tests with Pt-CNTs were repeated three times to check the reproducibility in the quantitative determination of the liquid compounds, obtaining errors lower than 3 %.

The products that we have identified, are mainly alcohols. The distribution profiles are very similar but with a slight increase of higher chain products for the Pt-doped TPE-CMP with CNTs in ratio 70–30 (wt%). However, testing the sample obtained by mixing Pt-doped CNTs (70 wt%) with TPE-CMP (30 wt%), isopropanol was one of the main products, confirming that the confinement effect due to the presence of the active phase (Pt nanoparticles) inside the CNTs, allowed the formation of the most stable tertiary carbon.

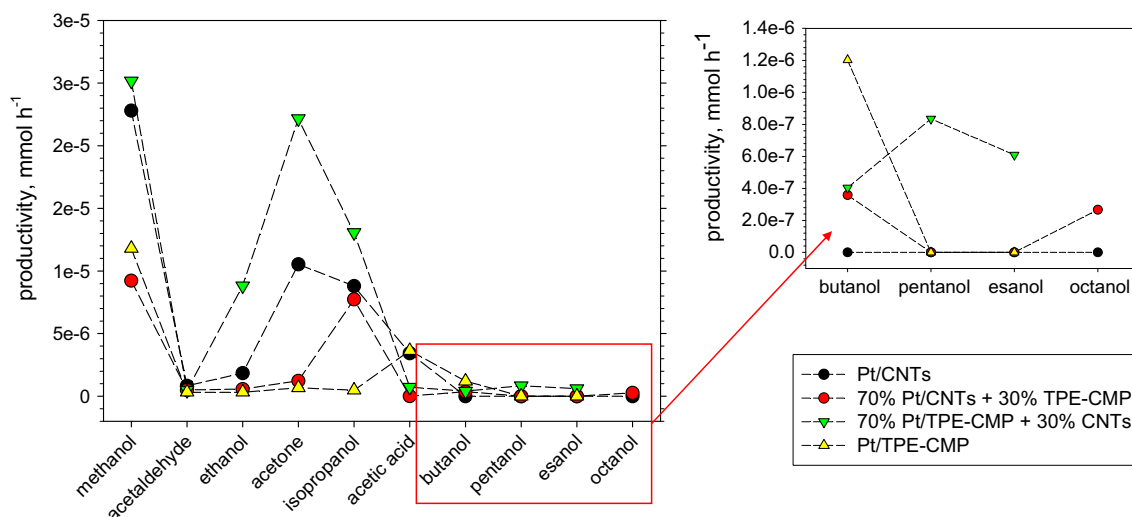
It is to notice that also higher chain hydrocarbons (until C8) were detected in all the testing experiments, but here we have limited our discussion to the more abundant liquid fractions of C1–C8 oxygenates (methanol, isopropanol, ethanol, acetic acid, acetaldehyde etc.) which we collected by using a cold trap. In the outlet gas flow we also detected hydrogen, carbon monoxide and methane. The faradic efficiency was also very high for all the tests (>95 %) even if the major part refers to the side reaction of water splitting.

The issue of the  $\text{H}_2$  production in gas phase electrocatalytic reduction of  $\text{CO}_2$  was discussed elsewhere [30].

### 3.3 Pt versus Fe

Avoiding the use of noble metals is an important further target to produce cheaper and environmental friendly electrode materials. In this view, we tested Fe-doped TPE-CMP electrocatalysts as well as Fe-doped CNTs as reference materials. The total productivities obtained for the Fe-doped samples are reported in Table 1. The productivities of the tests with Pt-doped CNTs and Pt-doped TPE-CMP mixed with CNTs are also reported as a comparison.

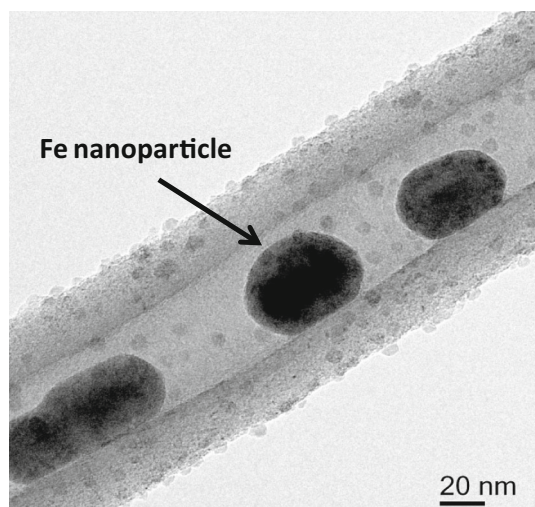
Unfortunately, at a first view results are not encouraging for Fe/TPE-CMP. As already discussed in Sect. 3.1, the deposition of metal nanoparticles (by sol-immobilization technique) on TPE-CMP led to particles with higher diameter for Fe with respect to Pt. Metal size and dispersion over the substrate surface play a fundamental role in the electrocatalytic performances in the process of  $\text{CO}_2$  reduction. The higher value of productivity obtained by testing Fe-doped CNTs with respect to Pt-doped CNTs, instead, depends on the confinement effect of Fe nanoparticles that well fit inside the CNTs (see Fig. 11), while for Pt-doped CNTs this effect is lower due to the different size and dispersion of the Pt nanoparticles inside the nanotubes [48]. The stability of the electrocatalysts in consecutive reaction cycles was also analysed. Results showed a higher deactivation rate for Fe-doped CNTs with respect to Pt-doped/CNTs. Further investigation is needed to improve the performances in the  $\text{CO}_2$  reduction process by using Fe-doped TPE-CMP as electrocatalytic material.



**Fig. 10** Distribution of the liquid products obtained in the gas-phase  $\text{CO}_2$  reduction process with Pt-doped TPE-CMP (CNTs) as electrocatalysts

**Table 1** Total productivity obtained in the gas-phase CO<sub>2</sub> reduction process using Fe-doped TPE-CMP (CNTs) as electrocatalysts

Electrocatalyst	Productivity (mmol h <sup>-1</sup> , e <sup>-5</sup> )
Fe/CNTs	6.1
70 % Fe/TPE-CMP + 30 % CNTs	2.5
Fe/TPE-CMP	1.7
Pt/CNTs	4.8
70 % Pt/TPE-CMP + 30 % CNTs	7.2

**Fig. 11** Representative TEM images of Fe-doped CNT electrocatalyst [48]

## 4 Conclusions

We reported here on the behaviour of conjugated microporous polymers (TPE-CMP) doped with Pt (or Fe) nanoparticles as electrocatalysts in the process of CO<sub>2</sub> reduction back to liquid fuels. The samples were prepared through Yamamoto homo-coupling reaction of a tetrahedral monomer, tetrakis (4-bromophenyl) ethene (TBPE), and then depositing on their surface Pt (or Fe) nanoparticles by sol immobilization technique.

The electrocatalytic materials were fully characterized and tested within our homemade electrochemical cell, working in gas phase, by applying a small bias between the working and counter electrodes. We described in detail the configuration and working of the electrocatalytic device and presented its advantages with respect to the more studied liquid phase electrochemical system (no problems of CO<sub>2</sub> solubility, no need to recover the liquid products, higher productivity and improved selectivity to high-chain hydrocarbons and oxygenates).

Results showed a relatively higher productivity by using the Pt-doped polymer as electrocatalyst, but it should be mixed to a small amount of CNTs to increase both the electronic conductivity and the quality of the ink before the impregnation on the C-based support. In the view of replacing noble metals, we also prepared and tested Fe-doped TPE-CMP electrocatalysts. Due to the different morphology and higher diameter of Fe nanoparticles with respect to Pt, Fe-doped electrocatalysts gave higher productivity only with CNTs as support, probably for the confinement effect occurring when Fe nanoparticles well fit inside the CNT. Further investigation is needed to improve their performances in the CO<sub>2</sub> reduction process, also exploiting different kinds of CMP synthesized from different monomers. However, these results are very promising and open new possibilities in the electrocatalytic conversion of CO<sub>2</sub> to liquid fuels by exploiting solar energy and closing the CO<sub>2</sub> cycle of its production/consumption.

**Acknowledgments** The authors would like to acknowledge the Italian Ministry of Education, University and Research (MIUR) for the financial support in the framework of the Project PRIN 2010–2011 (Mechanisms of CO<sub>2</sub> activation for the design of new materials for energy and resource efficiency).

## References

1. Centi G, Perathoner S, Passalacqua R, Ampelli C (2011) Solar production of fuels from water and CO<sub>2</sub>. In: (Eds.) NZMaTnV (ed) Carbon-neutral fuels and energy carriers. Series: green chemistry and chemical engineering. CRC Press (Taylor & Francis group), Boca Raton, FL (US), pp 291–323
2. Genovese C, Ampelli C, Perathoner S, Centi G (2013) A Gas-phase electrochemical reactor for carbon dioxide reduction back to liquid fuels. *Chem Eng Tran* 32:289–294. doi:10.3303/CET1332049
3. Songolzadeh M, Soleimani M, Takht Ravanchi M, Songolzadeh R (2014) Carbon dioxide separation from flue gases: a technological review emphasizing reduction in greenhouse gas emissions. *Sci World J* 2014:828131. doi:10.1155/2014/828131
4. Leung DY, Caramanna G, Maroto-Valer MM (2014) An overview of current status of carbon dioxide capture and storage technologies. *Renew Sustain Energy Rev* 39:426–443. doi:10.1016/j.rser.2014.07.093
5. Huck JM, Lin L-C, Berger AH, Shahrak MN, Martin RL, Bhowm AS, Haranczyk M, Reuter K, Smit B (2014) Evaluating different classes of porous materials for carbon capture. *Energy Environ Sci*. doi:10.1039/C4EE02636E
6. Yang L, Wang H (2014) Recent advances in carbon dioxide capture, fixation, and activation by using n-heterocyclic carbenes. *Chem Sus Chem* 7(4):962–998. doi:10.1002/cssc.201301131
7. Genovese C, Ampelli C, Perathoner S, Centi G (2013) Electrocatalytic conversion of CO<sub>2</sub> on carbon nanotube-based electrodes for producing solar fuels. *J Catal* 308:237–249. doi:10.1016/j.jcat.2013.08.026
8. Ampelli C, Centi G, Passalacqua R, Perathoner S (2010) Synthesis of solar fuels by a novel photoelectrocatalytic approach. *Energy Environ Sci* 3(3):292–301. doi:10.1039/B925470f

9. Ampelli C, Genovese C, Perathoner S, Centi G, Errahali M, Gatti G, Marchese L (2014) An electrochemical reactor for the CO<sub>2</sub> reduction in gas phase by using conductive polymer based electrocatalysts. *Chem Eng Trans* 41:13–18. doi:10.3303/CET1441003
10. Herron JA, Kim J, Upadhye AA, Hubera GW, Maravelias CT (2014) A general framework for the assessment of solar fuel technologies. *Energy Environ Sci*. doi:10.1039/C4EE01958J
11. Ampelli C, Genovese C, Passalacqua R, Perathoner S, Centi G (2012) The use of a solar photoelectrochemical reactor for sustainable production of energy. *Theor Found Chem Eng* 46(6): 651–657. doi:10.1134/S0040579512060012
12. Ampelli C, Passalacqua R, Perathoner S, Centi G (2011) Development of a TiO<sub>2</sub> nanotube array-based photo-reactor for H<sub>2</sub> production by water splitting. *Chem Eng Trans* 24:187–192. doi:10.3303/Cet1124032
13. Passalacqua R, Ampelli C, Perathoner S, Centi G (2012) Anodically formed TiO<sub>2</sub> thin films: evidence for a multiparameter dependent photocurrent-structure relationship. *Nanosci Nanotechnol Lett* 4(2):142–148. doi:10.1166/nl.2012.1303
14. Errahali M, Gatti G, Tei L, Canti L, Fraccarollo A, Cossi M, Marchese L (2014) Understanding methane adsorption in porous aromatic frameworks: an FTIR, Raman, and theoretical combined study. *J Phys Chem C* 118(19):10053–10060. doi:10.1021/jp412572e
15. Ampelli C, Passalacqua R, Genovese C, Perathoner S, Centi G, Montini T, Gombac V, Fornasiero P (2013) Solar energy and biowaste conversion into H<sub>2</sub> on CuO<sub>x</sub>/TiO<sub>2</sub> nanocomposites. *Chem Eng Trans* 35:583–588. doi:10.3303/CET1335097
16. Ampelli C, Passalacqua R, Genovese C, Perathoner S, Centi G, Montini T, Gombac V, Jaen JJD, Fornasiero P (2013) H<sub>2</sub> production by selective photo-dehydrogenation of ethanol in gas and liquid phase on CuO<sub>x</sub>/TiO<sub>2</sub> nanocomposites. *RSC Adv* 3(44): 21776–21788. doi:10.1039/C3ra22804e
17. You H-S, Jin H, Mo Y-H, Park S-E (2013) CO<sub>2</sub> adsorption behavior of microwave synthesized zeolite beta. *Mater Lett* 108:106–109. doi:10.1016/j.matlet.2013.06.088
18. Auta M, Hameed BH (2014) Adsorption of carbon dioxide by diethanolamine activated alumina beads in a fixed bed. *Chem Eng J* 253:350–355. doi:10.1016/j.cej.2014.05.018
19. Ye S, Jiang X, Ruan L-W, Liu B, Wang Y-M, Zhu J-F, Qiu L-G (2013) Post-combustion CO<sub>2</sub> capture with the HKUST-1 and MIL-101(Cr) metal-organic frameworks: adsorption, separation and regeneration investigations. *Microporous Mesoporous Mater* 179:191–197. doi:10.1016/j.micromeso.2013.06.007
20. Tong M, Yang Q, Xiao Y, Zhong C (2014) Revealing the structure-property relationship of covalent organic frameworks for CO<sub>2</sub> capture from postcombustion gas: a multi-scale computational study. *Phys Chem Chem Phys* 16(29):15189–15198. doi:10.1039/c4cp02047b
21. Ben T, Qiu S (2013) Porous aromatic frameworks: synthesis, structure and functions. *CrystEngComm* 15(1):17–26. doi:10.1039/c2ce25409c
22. Fraccarollo A, Canti L, Marchese L, Cossi M (2014) Monte carlo modeling of carbon dioxide adsorption in porous aromatic frameworks. *Langmuir* 30:4147–4156
23. Yang D-A, Cho H-Y, Kim J, Yang S-T, Ahn W-S (2012) CO<sub>2</sub> capture and conversion using Mg-MOF-74 prepared by a sonochemical method. *Energy Environ Sci* 5:6465–6473. doi:10.1039/c1ee02234b
24. Liu X, Li H, Zhang Y, Xu B, Sigen A, Xia H, Mu Y (2013) Enhanced carbon dioxide uptake by metalloporphyrin-based microporous covalent triazine framework. *Polym Chem* 4(8): 2445–2448. doi:10.1039/c3py00083d
25. Xu Y, Chen L, Guo Z, Nagai A, Jiang D (2011) Light-emitting conjugated polymers with microporous network architecture: interweaving scaffold promotes electronic conjugation, facilitates exciton migration, and improves luminescence. *J Am Chem Soc* 133(44):17622–17625. doi:10.1021/ja208284t
26. Xu Y, Jin S, Xu H, Nagai A, Jiang D (2013) Conjugated microporous polymers: design, synthesis and application. *Chem Soc Rev* 42(20):8012–8031. doi:10.1039/c3cs60160a
27. Xie Y, Wang TT, Liu XH, Zou K, Deng WQ (2013) Capture and conversion of CO<sub>2</sub> at ambient conditions by a conjugated microporous polymer. *Nature Commun* 4:1960. doi:10.1038/ncomms2960
28. Dawson R, Adams DJ, Cooper AI (2011) Chemical tuning of CO<sub>2</sub> sorption in robust nanoporous organic polymers. *Chem Sci* 2:1173–1177. doi:10.1039/c1sc00100k
29. Demir-Cakan R, Morcrette M, Nour F, Davoisne C, Devic T, Gonbeau D, Dominko R, Serre C, Ferey G, Tarascon J-M (2011) Cathode Composites for Li-S batteries via the use of oxygenated porous architectures. *J Am Chem Soc* 133(40):16154–16160. doi:10.1021/ja2062659
30. Genovese C, Ampelli C, Perathoner S, Centi G (2013) Electrocatalytic conversion of CO<sub>2</sub> to liquid fuels using nanocarbon-based electrodes. *J Energy Chem* 22(2):202–213
31. Ampelli C, Passalacqua R, Genovese C, Perathoner S, Centi G (2011) A novel photo-electrochemical approach for the chemical recycling of carbon dioxide to fuels. *Chem Eng Trans* 25: 683–688. doi:10.3303/Cet1125114
32. Ampelli C, Passalacqua R, Perathoner S, Centi G, Su DSS, Weinberg G (2008) Synthesis of TiO<sub>2</sub> Thin films: relationship between preparation conditions and nanostructure. *Top Catal* 50(1–4):133–144. doi:10.1007/s11244-008-9113-0
33. Ampelli C, Passalacqua R, Perathoner S, Centi G (2009) Nano-engineered materials for H<sub>2</sub> production by water photo-electrolysis. *Chem Eng Trans* 17:1011–1016. doi:10.3303/Cet0917169
34. Kuhl KP, Cave ER, Abram DN, Jaramillo TF (2012) New insights into the electrochemical reduction of carbon dioxide on metallic copper surfaces. *Energy Environ Sci* 5(5):7050. doi:10.1039/c2ee21234j
35. Ampelli C, Genovese C, Passalacqua R, Perathoner S, Centi G (2014) A gas-phase reactor powered by solar energy and ethanol for H<sub>2</sub> production. *Appl Therm Eng* 70(2):1270–1275. doi:10.1016/j.applthermaleng.2014.04.013
36. Kopljar D, Inan A, Vindayer P, Wagner N, Klemm E (2014) Electrochemical reduction of CO<sub>2</sub> to formate at high current density using gas diffusion electrodes. *J Appl Electrochem* 44(10): 1107–1116. doi:10.1007/s10800-014-0731-x
37. Wang Q, Dong H, Yu H, Yu H (2015) Enhanced performance of gas diffusion electrode for electrochemical reduction of carbon dioxide to formate by adding polytetrafluoroethylene into catalyst layer. *J Power Sources* 279:1–5. doi:10.1016/j.jpowsour.2014.12.118
38. Ampelli C, Perathoner S, Centi G (2015) CO<sub>2</sub> utilization: an enabling element to move to a resource and energy-efficient chemical and fuel production. *Phil Trans R Soc A* 373 (20140177):1–35. doi:10.1098/rsta.2014.0177
39. Qiao J, Liu Y, Hong F, Zhang J (2014) A review of catalysts for the electroreduction of carbon dioxide to produce low-carbon fuels. *Chem Soc Rev* 43:631–675. doi:10.1039/c3cs60323g
40. Wang D, Villa A, Porta F, Su D, Prati L (2006) Single-phase bimetallic system for the selective oxidation of glycerol to glycerate. *Chem Commun* 18:1956–1958. doi:10.1039/B518069D
41. Freund H-J, Roberts MW (1996) Surface chemistry of carbon dioxide. *Surf Sci Rep* 25(8):225–273. doi:10.1016/S0167-5729(96)00007-6
42. Fastow M, Kozirovski Y, Folman M (1993) IR spectra of CO<sub>2</sub> and N<sub>2</sub>O adsorbed on C<sub>60</sub> and other carbon allotropes—a comparative study. *J Electron Spectrosc Relat Phenom* 64–65(C): 843–848. doi:10.1016/0368-2048(93)80158-I

43. Mawhinney DB, Rossin JA, Gerhart K, Yates JT Jr (1999) Adsorption and reaction of 2-chloroethylethyl sulfide with  $\text{Al}_2\text{O}_3$  surfaces. *Langmuir* 15(14):4789–4795. doi:[10.1021/la981440v](https://doi.org/10.1021/la981440v)
44. Kazarian SG, Vincent MF, Bright FV, Liotta CL, Eckert CA (1996) Specific intermolecular interaction of carbon dioxide with polymers. *J Am Chem Soc* 118(7):1729–1736. doi:[10.1021/ja950416q](https://doi.org/10.1021/ja950416q)
45. Matranga C, Chen L, Smith M, Bittner E, Johnson JK, Bockrath B (2003) Trapped  $\text{CO}_2$  in Carbon Nanotube Bundles. *J Phys Chem B* 107(47):12930–12941
46. Hori Y (2008) Electrochemical  $\text{CO}_2$  reduction on metal electrodes. In: Constantinos G, Vayenas C, White RE, Gamboa-Aldeco ME (eds) *Modern aspects of electrochemistry*, vol 42. Springer, New York, pp 89–189. doi:[10.1007/978-0-387-49489-0\\_3](https://doi.org/10.1007/978-0-387-49489-0_3)
47. Ampelli C, Perathoner S, Centi G (2014) Carbon-based catalysts: opening new scenario to develop next-generation nano-engineered catalytic materials. *Chin J Catal* 35(6):783–791. doi:[10.1016/S1872-2067\(14\)60139-X](https://doi.org/10.1016/S1872-2067(14)60139-X)
48. Gangeri M, Perathoner S, Caudo S, Centi G, Amadou J, Bégin D, Pham-Huu C, Ledoux MJ, Tessonnier JP, Su DS (2009) Fe and Pt carbon nanotubes for the electrocatalytic conversion of carbon dioxide to oxygenates. *Catal Today* 143(1–2):57–63. doi:[10.1016/j.cattod.2008.11.001](https://doi.org/10.1016/j.cattod.2008.11.001)